J Supercond Nov Magn (2013) 26:2831–2835
DOI 10.1007/s10948-013-2263-8

ORIGINAL PAPER

Normal and Superconducting Properties of Cuprates in Multielectron Theory

Sergey Ovchinnikov · Maxim Korshunov · Sergey Nikolaev · Elena Shneyder · Aleksandr Krinitsyn

Received: 2 May 2013 / Accepted: 8 May 2013 / Published online: 31 May 2013
© Springer Science+Business Media New York 2013

Abstract We consider the doping dependence of the normal and superconducting properties of $La_{2-x}Sr_xCuO_4$ in the low energy effective model based on the ab initio LDA+GTB calculations. We have found that two quantum phase transitions (QPT) of the Lifshitz type correspond well to the experimental phase diagram. For superconducting state, we have considered both magnetic and phonon mechanisms of pairing. Finally, we compare the true Fermi surface and the spectral intensity map seen in ARPES within a new norm conserving cluster perturbation theory (NC-CPT).

Keywords Strong electron correlations · Fermi surface reconstruction · Cluster perturbation theory

S. Ovchinnikov (✉) · M. Korshunov · E. Shneyder
Kirensky Institute of Physics, Siberian Branch, Russian Academy of Sciences, Krasnoyarsk, 660036, Russia
e-mail: sgo@iph.krasn.ru

E. Shneyder
e-mail: shneyder@iph.krasn.ru

S. Ovchinnikov · M. Korshunov · S. Nikolaev
Siberian Federal University, Krasnoyarsk 660041, Russia

S. Nikolaev
e-mail: 25sergeyn@mail.ru

E. Shneyder
Reshetnev Siberian State Aerospace University, Krasnoyarsk 660014, Russia

A. Krinitsyn
Dostoyevsky Omsk State University, Omsk 644077, Russia
e-mail: krinitss@mail.ru

1 Introduction

Effects of strong electron correlations (SEC) hinder the conventional LDA method from the correct description the electronic structure of $La_{2-x}Sr_xCuO_4$ in a wide range of doping from the underdoped antiferromagnetic (AFM) insulator to the overdoped normal Fermi liquid. The multielectron LDA+GTB approach has been developed in our group [1, 2] to calculate the quasiparticle band structure with SEC being incorporated. To study doping dependence of the Fermi surface the k-dependence of the self-energy due to the short AFM order is crucial [3]. This dependence results in two QPT between underdoped and overdoped region [4]. The first one at $x_{c1} = 0.15$ accompanies with the logarithmic singularity of the density of state (DOS) at the Fermi level; the second one at $x_{c2} = 0.24$ results in the step singularity of the DOS [5].

In this paper, we analyze the effect of QPT on the phase diagram in the normal and superconducting state. Due to importance of the AFM short range order, we have developed a new approach to the cluster perturbation theory, the NC-CPT [6]. Here, we compare the Fermi surface resulting from the Green function pole and the spectral intensity map for different concentrations and linewidth within the NC-CPT method.

2 Effect of the Quantum Phase Transitions on the Phase Diagram

An electron in SEC material within the LDA+GTB method is a linear superposition of the Hubbard fermions. Each fermion is a quasiparticle that corresponds to the excitation of the initial multielectron term d_i^n with the energy $E_i(n)$ into the final term d_j^{n+1} with the energy $E_j(n+1)$. These

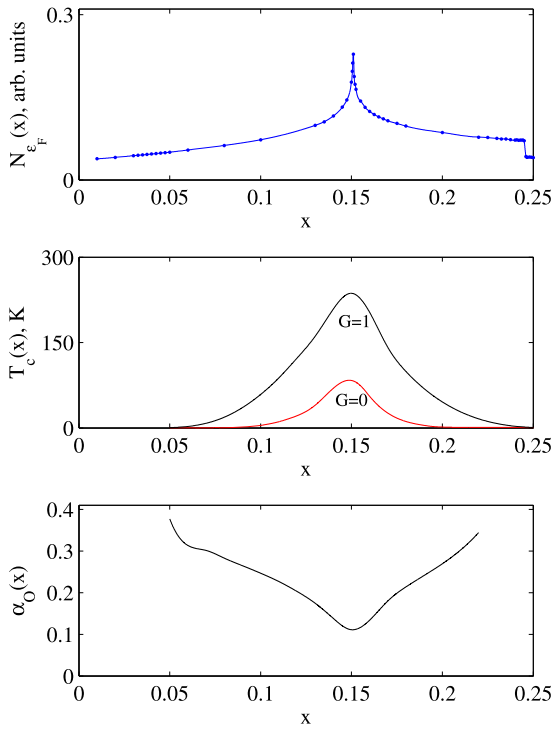

Fig. 1 The concentration dependence of the Fermi level density of states, T_c, and isotope effect. *Two curves* for T_c corresponds to pure magnetic pairing ($G = 0$) and magnetic and phonon pairing ($G = J$)

terms and energies are obtained by the exact diagonalization of the multielectron Hamiltonian inside the unit cell. The local quasiparticle energy is equal to $\Omega_{ij} = E_i(n+1) - E_i(n)$. The intercell hopping results the dispersion $\Omega_{ij} \to \Omega_{ij}(k)$.

We treat the intercell hopping as the perturbation. A simplest version of the perturbation theory is given by the Hubbard 1 approximation. Beyond it, there are spin fluctuations. The self-energy was calculated [3] in the non-crossing approximation by neglecting vertex renormalization that is equivalent to the self-consistent Born approximation (SCBA) [7].

The concentration dependence of the electronic structure results in the change the Fermi surface topology from the small hole pocket centered near $(\pi/2, \pi/2)$ at $x < x_{c1}$ to the large hole and small electronic pockets around (π, π) at $x > x_{c1}$. The electronic pocket collapses at x_{c2}, and at $x > x_{c2}$ there is only large hole Fermi surface [4, 5].

We have considered here the thermodynamics of the normal and superconducting phases as function of doping concentration. We have found a remarkable kink in the kinetic energy in the normal state at $T = 0$ $E_{\rm kim}(x)$ dependence at $x = x_{c2}$. Above x_{c2} $E_{\rm kim}(x)/E_{\rm kim}(x_{c2}) \approx 1 + x$, which is expected for a conventional 2D metal with hole concentration $n_h = 1 + x$. Below x_{c2}

$$E_{\rm kim}(x)/E_{\rm kim}(x_{c2}) = \exp\bigl[-4E_g(p)/J\bigr],$$

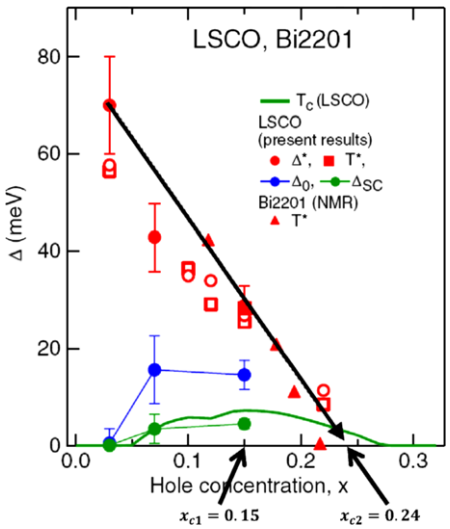

Fig. 2 The concentration dependence of the two characteristic energy scales T_c and T^* from [12] and two critical points from our calculations

where J is the exchange coupling and $E_g = J(x_{c2} - x)/x_{c2}$ is a doping dependent pseudogap.

The mean field theory of superconductivity of the Hubbard fermions with simultaneous magnetic and phonon mechanisms of pairing [8] has been developed similar to the d-wave pairing theory in the strongly correlated regime of the Hubbard model [9]. We have found that the log singularity at x_{c1} results both in the maximum of the critical temperature T_c and minimum in the isotope effect exponent α (Fig. 1).

We have compared the experimental phase diagram of the single CuO_2 layer cuprates with our calculated QPT critical points (Fig. 2). The optimal doping is determined by x_{c1}. The extrapolation of the pseudogap temperature $T^*(x) \to 0$ gives $T^*(x_{c2}) = 0$. Thus, both our calculations of the energy and comparison with $T^*(x)$ dependence allow us to conclude that x_{c2} is the critical point separated the Fermi liquid $x > x_{c2}$ and non-Fermi liquid (pseudogapped) at $x < x_{c2}$ regimes.

3 Comparison of the Fermi Surface and Spectral Intensity Map

There are a lot of experimental evidences from ARPES about weakly doping dependent Fermi arc [10]. The two QPT picture seems to contradict such data. The Fermi surface discussed above results from the poles of the Green function, while the ARPES measures the momentum distribution curves that are proportional to the spectral intensity map under assumption of the constant matrix elements. In this section, we calculate both the poles and spectral intensity maps for the hole doped Hubbard model within the NC-CPT approach [6]. It is the new version of the cluster

perturbation theory (CPT) with exact diagonalization of the cluster and perturbation treatment of the intercluster hopping in the X-operator representation.

We consider the one-band two-dimensional Hubbard model

$$H = \sum_{i\sigma} \left\{ (\varepsilon - \mu) n_{i\sigma} + \frac{U}{2} n_{i\sigma} n_{i\bar{\sigma}} \right\} + \sum_{i \neq j, \sigma} t_{ij} a^{\dagger}_{i\sigma} a_{j\sigma}, \quad (1)$$

where ε is the energy of an electron at a site, μ is the chemical potential, U is the parameter of the Coulomb interaction at a site, t_{ij} is the hopping integral, $a^{\dagger}_{i\sigma}$ and $a_{i\sigma}$ are the creation and annihilation operators for an electron with spin σ at site i, $\bar{\sigma} = -\sigma$, $n_{i\sigma} = a^{\dagger}_{i\sigma} a_{i\sigma}$.

Let us to break down the lattice on the clusters. After that we can separate the intra and intercluster interactions

$$H = \sum_{f} H_0(f) + \sum_{f \neq g} H_t(f, g), \quad (2)$$

where f, g are the cluster indexes.

We determine the complete set of exact eigenvectors and eigenvalues of the intracluster part of the Hamiltonian (2) by the exact diagonalization method. The complete basis allows us to construct X-operators for cluster and rewrite the initial lattice Hamiltonian to the cluster Hamiltonian in the X-representation. The Green function is obtained by the perturbation method. The simplest non-trivial solution is given by the Hubbard 1 approximation. In framework of this approach, we have suggested the norm-conserving version of CPT and determine the value (f-factor) [6], which allows us to control the spectral weight of Hubbard fermions.

Our calculations have shown that the spectral weight of the in-gap states is increased with the hole concentration due to the spectral weight of the upper Hubbard band (UHB). The position of the in-gap states dependents on a value of the Coulomb repulsion U. In particular, for $U = 8t$ these states appear near the lower Hubbard band (LHB), and near the UHB at $U = 2t$.

The study has revealed the presence of the pseudogap state and a nonuniform distribution of the quasiparticle spectral weight along the Fermi surface. We have obtained a cascade of QPT with increasing hole concentration. In the case of nonzero nonnearest hopping, the Fermi surface has the form of arc (Fig. 3) in agreement with ARPES data.

In the Fig. 4, we plot the Fermi surface and spectral intensity map for 3 different concentrations. For undoped region $x = 0.0025$, we have a small hole pocket and line of zeros. Calculating the spectral intensity usually a small finite linewidth δ is introduced that models the experimental resolution. The value $\delta/t = 0.1$ results in a transformation of the pocket into the arc (Fig. 4c), while better resolution $\delta/t = 0.01$ results in the map very close to the Fermi surface similar to the cellular DMFT plus exact diagonalization method [11]. With increasing doping the smaller pocket

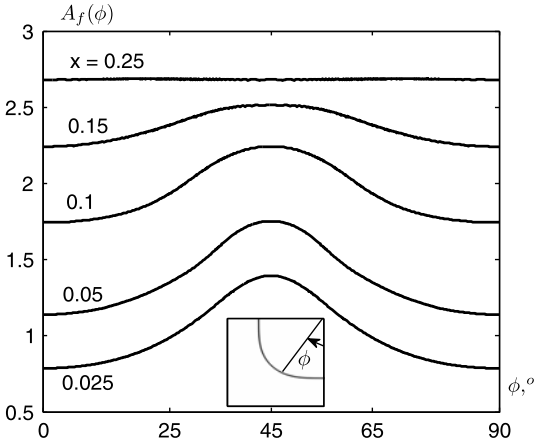

Fig. 3 The spectral weight along the Fermi surface A_f vs. the angle ϕ for hole doping $x = 0.025, 0.05, 0.1, 0.15, 0.25$. Here, $\phi = 0^0$ responds the antinodal direction $((\pi, 0) \rightarrow (\pi, \pi))$, $\phi = 45^0$ is the nodal direction $((0, 0) \rightarrow (\pi, \pi))$. The model parameters [3]: $U = 2.15t$, $t' = -0.13t$, $t'' = 0.16t$. The linewidth parameter $\delta = 0.1t$

around (π, π) meets the line of zeros and they mutually annihilated. In the Fermi liquid regime at $x = 0.20$, all three columns show the same Fermi surface. We have shown that the broadening washes out picture of the Lifshitz transition and results in smooth filling the pseudogap (see Fig. 3).

The dispersion curves along symmetric directions are in good agreement with other works. It was shown that in the nodal direction the dispersion curve is divided into sections with different slopes separated by gaps. As we ignore the phonon component, the difference in the slope associated with interaction in the electronic subsystem. Thus, the kinks observed in experiments can result from the electron-electron interactions that lead to a distortion of the dispersion curve. This conclusion is consistent with the results of [13].

The next step we chose the clusters with shapes shown in Fig. 5. These clusters can be divided into two types. The first type of clusters (Fig. 5a, c) consists of sites with the same number of nearest neighbors, i.e., sites of the same type. The second type clusters (Fig. 5b, d, e) consisting of two types of sites with different number of nearest neighbors. For example, the cluster in Fig. 5b shows sites 2 and 3 of same type with the number of nearest neighbors equaling 1 and site 1 of the other type with two nearest neighbors, i.e., attributed to the second type.

The paper [6] describes the study of the band structure for 4-sites cluster (Fig. 5c) in which the band is split into two Hubbard bands for half filling and $U = 8t$. We have performed calculations for 5-sites cluster (Fig. 5e), which showed that in this case the additional splitting of each Hubbard band into two subbands occurs. The similar situation was observed in paper [14], in which the authors carried out the calculations by means of the quantum Monte-Carlo

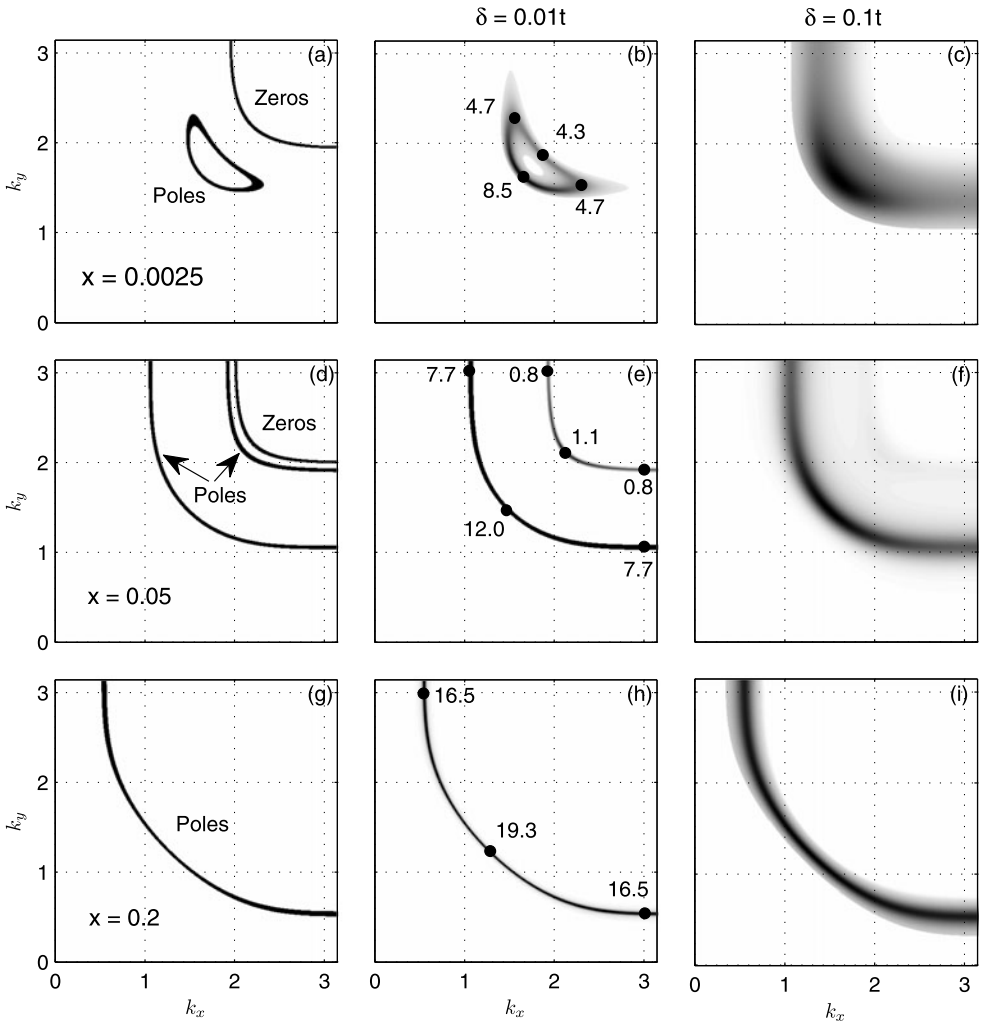

Fig. 4 The Fermi surface in three concentration regions from poles of the Green function (**a**, **d**, **g**) and spectral intensity map for high (**b**, **e**, **h**) and low (**c**, **f**, **i**) resolution. The numbers in (**b**, **e**, **h**) show the spectral intensity for a given k-point

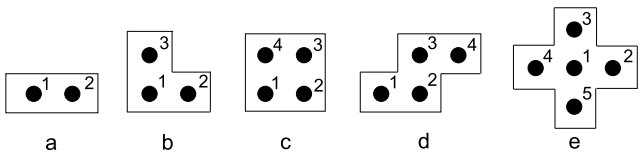

Fig. 5 Cluster shapes

method. This difference in the band structures of 4- and 5-sites clusters could be explained either by taking into account the long-range spatial correlations within the cluster or its symmetry.

We have obtained a band structure with the 3-sites cluster (Fig. 5b) similar to the band structure of the 5-sites cluster. Figure 6 shows the density of states for the three types of clusters (Fig. 5b, c, e), where this analogy (the gap in the vicinity $\omega = \pm 4t$) as well as the contrast with the band structure with the 4-sites cluster are clearly seen. The study excludes the interpretation of the Hubbard bands splitting by the presence of long-range spatial correlations from the intracluster interactions.

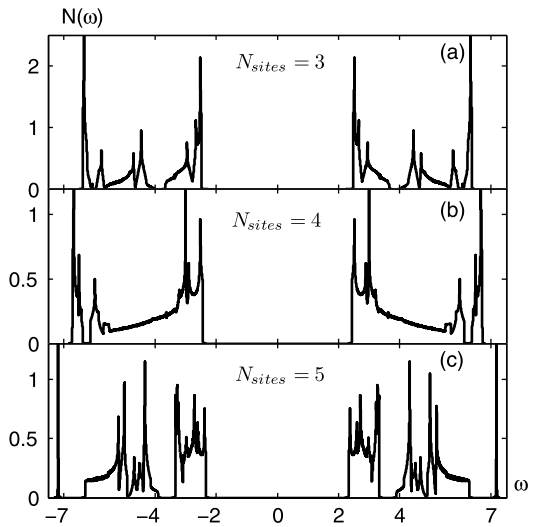

Fig. 6 The density of states of the 3-sites (**a**), 4-sites (**b**) and 5-sites (**c**) clusters for $U = 8t$, $f > 0.95$. The linewidth parameter $\delta = 0.001t$

Additional band structure calculations for the two cluster shapes (Fig. 5a, d) allowed us to exclude the effect of the

cluster sites parity. Thus, the splitting of the Hubbard bands is determined by the presence of different kinds of sites in the cluster.

Acknowledgements This work is supported by Grants NS-1044. 2012.2, MK-1168.2012.2, RFFI grant 13-02-01395, GK 16.740.12. 0731, Project SORAN 44, Siberian Federal University F11, Dynasty Foundation.

References

1. Gavrichkov, V.A., Ovchinnikov, S.G., Borisov, A.A., Goryachev, E.G.: J. Exp. Theor. Phys. **91**, 369 (2000)
2. Korshunov, M.M., Gavrichkov, V.A., Ovchinnikov, S.G., Pchelkina, Z.V., Nekrasov, I.A., Korotin, M.A., Anisimov, V.I.: J. Exp. Theor. Phys. **99**, 559 (2004)
3. Korshunov, M.M., Ovchinnikov, S.G.: Eur. Phys. J. B **57**, 271 (2007)
4. Ovchinnikov, S.G., Korshunov, M.M., Shneyder, E.I.: J. Exp. Theor. Phys. **109**, 775 (2009)
5. Ovchinnikov, S.G., Shneyder, E.I., Korshunov, M.M.: J. Phys. Condens. Matter **23**, 045701 (2011)
6. Nikolaev, S.N., Ovchinnikov, S.G.: J. Exp. Theor. Phys. **111**, 634 (2010)
7. Plakida, N.M., Oudovenko, V.S.: J. Exp. Theor. Phys. **104**, 230 (2007)
8. Ovchinnikov, S.G., Shneyder, E.I.: J. Supercond. Nov. Magn. **23**, 733 (2010)
9. Plakida, N.M., Oudovenko, V.S.: Phys. Rev. B **59**, 11949 (1999)
10. Kordyuk, A.A., Borisenko, S.V., Knupfer, M., Fink, J.: Phys. Rev. B **67**, 064504 (2003)
11. Sakai, S., Motome, Y., Imada, M.: Phys. Rev. Lett. **102**, 056404 (2009)
12. Yoshida, T., et al.: Phys. Rev. Lett. **137**, 037004 (2009)
13. Byczuk, K., Kollar, M., Held, K., Yang, Y.-F., Nekrasov, I.A., et al.: Nat. Phys. **3**, 168 (2007)
14. Grober, C., Eder, R., Hanke, W.: Phys. Rev. B **62**, 4336 (2000)